Tin-Based Perovskite Solar Cells: Optimization via Bulk and Interfacial Engineering

A Thesis

Presented to the Faculty of the Graduate School

of Cornell University

In Partial Fulfillment of the Requirements for the Degree of

Master of Science

by

Ningyuan Zhang

August 2025

ABSTRACT

Tin-based perovskite solar cells (TPSCs) have emerged as promising alternatives to lead-based devices due to their reduced toxicity and favorable optoelectronic properties. However, challenges such as Sn^{2+} oxidation, poor film morphology, and inefficient charge extraction continue to limit their broader application. This work presents a comprehensive approach that integrates bulk and interfacial engineering to address these challenges in quasi-two-dimensional/three-dimensional (2D/3D) TPSCs. We focused on the tin perovskite bulk, introducing additives to both precursor and antisolvent to improve phase distribution inside the perovskite film and modulate its crystallization kinetics. We further implemented dual interfacial modifications—employing organic spacer ligands at the bottom to regulate the nucleation and growth of the perovskite films, and fullerene-based surface treatments at the top to improve energy level alignment and enhance electron extraction. The results show remarkable improvements in photovoltaic performances. These complementary strategies collectively establish a unified framework for improving tin perovskite solar cell performance through rational molecular and interface design.

BIOGRAPHICAL SKETCH

Ningyuan Zhang received his B.S. degree in Materials Science and Engineering from Guangdong Technion – Israel Institute of Technology (GTIIT) in 2023. He conducted research on solid-state dewetting of copper thin film under the direction of Professor Yuanshen Qi, focusing on the microstructure change of metal thin films driven by surface energy minimization under high temperature. In 2023, he joined the Master's program in Materials Science and Engineering at Cornell University and became Professor Qiuming Yu's research group member, studying the bulk and interface modification in tin-based perovskite solar cells.

ACKNOWLEDGMENTS

Sincere appreciation to my advisors Professor Qiuming Yu and Professor Yu Zhong. Also to my group members Baitao Chen, Xiaoyu Zhang, Adewale Babatunde, Taiyi Chen, Yuanze Xu, Shripathi Ramakrishnan, Chenwei Zhu, Letian Li, Xinyu Yin, and Xiaozhou Zheng for their guidance, encouragement, and other valuable support.

TABLE OF CONTENTS

LIST OF FIGURES

LIST OF TABLES

CHAPTER 1

INTRODUCTION

Energy has always been a fundamental topic throughout human history. In the past, our society largely relied on non-renewable sources such as fossil fuels. However, concerns about sustainability and environmental impact have made the transition to renewable energy increasingly urgent. Over the past two decades, the global renewable energy capacity has grown rapidly, from 753 gigawatts in 2000 to approximately 2799 gigawatts by 2020. According to the prediction, by 2050, around 86% of the world's electricity is expected to come from renewable sources.

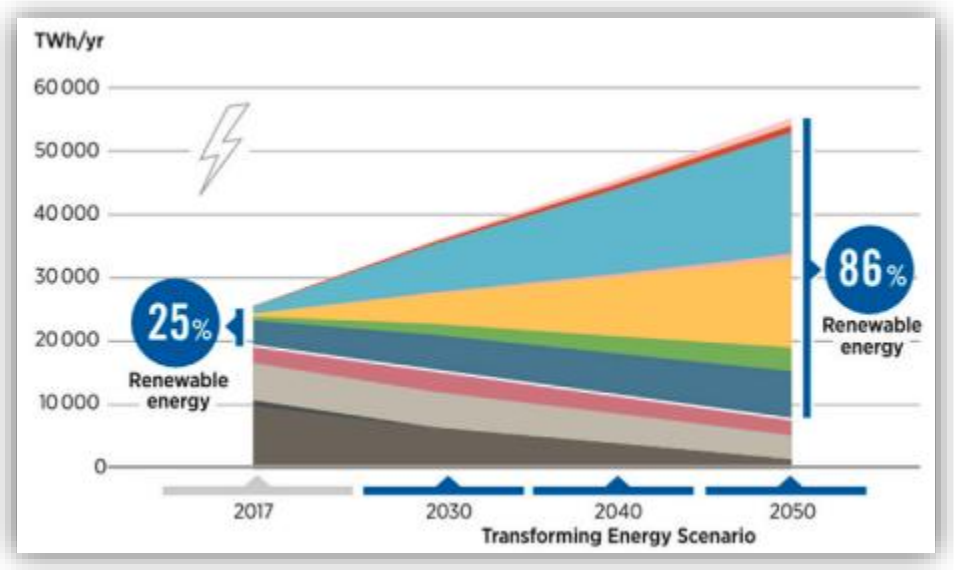

Figure 1.1 World electricity generation and predictions by 2050. [1]

Among the renewable energy sources, solar energy has shown the fastest growth rate. Metal halide perovskite solar cells (PSCs) have garnered tremendous attention due to their remarkable optoelectronic properties of perovskites and rapidly increasing power conversion efficiencies (PCEs). Among them, lead-based perovskites have dominated the field with top solar cell performance, yet concerns over the intrinsic toxicity of lead and its potential environmental hazards have driven the pursuit of safer alternatives. Tin-based perovskites, featuring a similar electronic structure and a more environmentally friendly, have been considered as one of the most promising candidates to replace lead in next-generation PSCs. In addition to being non-toxic, tin-

based perovskites offer a narrower bandgap and good carrier mobility, which theoretically supports high-efficiency photovoltaic performance.

Despite these advantages, the development of efficient tin-based PSCs remains challenging. Devices based on tin perovskites typically suffer from low open-circuit voltage (V_{OC}) and moderate stability over oxidation, significantly lagging behind their lead-based counterparts. The easy oxidation nature of tin comes from the active 5s electrons and the fast crystal growth comes from the strong electrophilicity on 5p orbital [2]. These shortcomings are largely attributed to the intrinsic instability of Sn^{2+}, which tends to oxidize to Sn^{4+} under ambient conditions, introducing self-doping and accelerating non-radiative recombination. Furthermore, the rapid crystallization kinetics of tin halide precursors often lead to poor film morphology with high defect density, pinholes, and small grain sizes. Addressing these issues is critical to reach the full potential of tin-based PSCs and closing the performance gap with lead-based systems. Therefore, significant research efforts have been directed towards improving film quality, suppressing oxidation, and enhancing interfacial engineering through additive strategies, dimensional modulation, and compositional design.

One promising direction involves the use of 2D tin perovskites, where organic spacer cations are introduced into the 3D framework, segmenting the structure into lower-dimensional components. This modification enhances device stability by forming layered structures that resist moisture and oxygen infiltration. However, the resulting multiple quantum- well (MQW) structure introduces new challenges—most notably high exciton binding energies and hindered charge transport due to alternating organic/inorganic layers. These characteristics necessitate precise control over the composition, dimensionality, and spatial distribution of the perovskite phases.

To address these issues, this research explores a combination of structural and interfacial engineering strategies aimed at enhancing the performance of 3D/2D tin PSC perovskite solar cells. Specific approaches include exploring hole transport materials with high extraction efficiency, optimizing the perovskite film through compositional tuning (e.g., incorporating methylammonium bromide (MABr), ammonium thiocyanate (NH_4SCN), and guanidinium thiocyanate (GASCN)), adjusting device layer thicknesses, and implementing low-dimensional interlayers at the bottom of the active layer to orient crystal growth and passivate defects.

CHAPTER 2

EXPERIMENTAL METHODS

2.1 Materials

Tin powder (Sn, 99.8%), iodine (I_2, 99.99%), tin fluoride (SnF_2, 99%), chlorobenzene (CB, 99.8%, anhydrous), N-dimethylformamide (DMF, 99.8%, anhydrous), dimethyl sulfoxide (DMSO, 99.9%, anhydrous), toluene (99.8%, anhydrous), bathocuproine (BCP, 99.99%) were purchased from Sigma-Aldrich. 6-phosphonohexanoic acid (6PA, 97%), [2-(3,6-Dimethoxy-9H-carbazol-9-yl)ethyl]phosphonic acid (MeO-2PACz, TCI), ammonium thiocyanate (NH4SCN, > 97.5%), methylammonium bromide (MABr, 99.99%), guanidinium thiocyanate (GASCN 99.8%), [6,6]-phenyl C61 butyric acid methyl ester (PCBM, > 99.9%) and indene-C60 bisadduct (ICBA, > 99.9%) were purchased from Nano-C (Massachusetts, USA). Phenethylammonium iodide (PEAI), 4-fluorophenethylammonium iodide (4-FPEAI, 99%), Phenethylammonium thiocyanate (PEASCN), and 2-Thiopheneethylammonium iodide (2-TEAI) were purchased from GreatCell (Queanbeyan, Australia). PEDOT: PSS (Clevios™ P VP Al 4083) was purchased from Heraeus.

2.2 Fabrication of Tin Perovskite Films

Iodide 475 mg and tin powder 375 mg were dissolved in the mixed solvent of 353 µl DMSO and 1412 µl DMF to obtain the 1M SnI_2 solution. The resulting solution (400 µl) was mixed with formamidinium iodide (FAI) 58.5 mg, phenethylammonium iodide (PEAI) 15 mg and SnF_2 6.25 mg. The solution was then heated at 70 °C for 1.5 h before use. 65 µl of the PEDOT: PSS was dropped on cleaned ITO glasses and spin-coated at 4500 rpm for 45 s and annealed at 150 °C for 20 min The precursor was deposited onto the PEDOT: PSS/ITO substrate via a spin-coating process at 1000 rpm for 10 s and 5000 rpm 30 s in a N_2-filled glove box. During the spin-coating, 200 µl chlorobenzene or 500 µl toluene was dropped onto the spinning substrate. The films were obtained after thermal annealing at 70 °C for 10 min.

2.3. Fabrication of Tin Perovskite Solar Cells

The ITO substrates were ultrasonically cleaned with detergent (diluted), deionized water, acetone, and isopropanol for 20 min each. Then, the as-cleaned ITO substrates were treated by oxygen plasma at high power for 15 min. PEDOT: PSS was spin-coated onto the cleaned ITO

substrate at 4500 rpm for 40 s and annealed at 150 °C for 20 min. The coated substrate was transferred to the glove box after cooling down to room temperature. For the devices with co-SAM as the hole transport, 0.3 mg/ml MeO-2PACz and 6PA were separately dissolved in ethanol and sonicated for 30 min. Then two solutions were mixed in equal volume to obtain the co-SAM solution. The mixed solution was dropped on clean ITO surfaces and rested for 15 seconds, followed by spin-coating at 3000 rpm for 30 s. The film was then annealed at 100 °C for 10 min. For the device with organic ligand bottom treatments, the organic ligands were dissolved in DMF and spin-coated onto the PEDOT: PSS layer at 3000 rpm for 30 s. Subsequently, the perovskite precursor solution was deposited onto the substrate via a spin-coating process at 1000 rpm for 10 s and 5000 rpm for 30 s. During the spin-coating, 200 μl chlorobenzene or 500 μl toluene was dropped onto the spinning substrate at the 8th second of stage two. The films were obtained after thermal annealing at 70 °C for 10 min. Then, for the control device, PCBM 30 mg/ml in chlorobenzene was sequentially spin-coated onto the perovskite layer at 1500 rpm for 30 s and then annealed at 70°C for 10 min. BCP 0.5 mg/ml in IPA was then spin-coated at 5000 rpm for 40 s. Finally, silver electrode (100 nm) was thermally evaporated in the vacuum chamber at 2 Å/s under a vacuum of $<10^{-7}$ torr.

2.4. Characterization of Tin Perovskite Solar Cells

The current density–voltage (J–V) characterizations were conducted in a N_2-filled glovebox with a SS-F5-3A Solar Simulator (EnliTech). The opening area of 0.0324 cm^2 was set by the mask and the light intensity was calibrated to 100 mW/cm^2.

2.5. Characterization of Tin perovskite films

UV-Vis absorption spectra were obtained by a UV-Vis-NIR spectrometer (Varian Cary 5000). Ex-situ GIWAXS tests were conducted in Brookhaven National Laboratory.

CHAPTER 3

Bulk Engineering via Additives and Gradient Annealing

2D/3D perovskite solar cells have gained increasing attention due to their improved environmental stability and tunable optoelectronic properties. However, the alternating organic-inorganic layered structure in 2D perovskites often results in complex phase distributions with mixed quantum-well behavior, and the formation of undesirable low-n phases (e.g., n = 1) remains a key limitation to charge transport and efficiency. These low-dimensional phases typically act as barriers to vertical carrier transport and lead to increased charge carrier recombination, limiting device performance. Therefore, developing effective strategies to modulate phase distribution within the perovskite thin films matrix is essential for achieving higher power conversion efficiencies.

3.1 Polymer Additives

Polymers have played versatile roles in the engineering of perovskite solar cells, including use as precursor additives, antisolvent components, interfacial layers, and surface treatments. In our system, we have tried to incorporate the polymethylmethacrylate (PMMA) (Figure 3.1). When incorporated into the perovskite, PMMA is hypothesized to interact with organic cations such as formamidinium via hydrogen bonding and with Sn^{2+} via Lewis acid-base interaction. These interactions enable PMMA to serve as a passivating agent, reducing trap state density at grain boundaries, promoting more uniform film morphology, and mitigating Sn^{2+} oxidation.

We tried to incorporate PMMA into both precursor and antisolvent. Direct PMMA addition in the precursor causes obvious phase separation in the film, as shown in Figure 3.1b. Severe phase separation was shown after annealing process, which has destroyed the whole film. To address this issue, PMMA was then used together with the antisolvent. Different concentrations of PMMA were dissolved in chlorobenzene (CB) and dropped during the spin coating process at the last 8 s of the second spin-coating process. The device performance was summarized in Table 3.1.

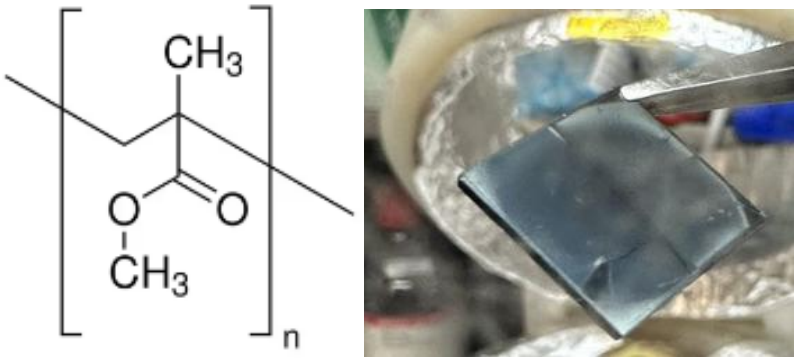

Figure 3.1 (a) Chemical structure of PMMA. (b) Photograph of a spin-coated perovskite film with 20 mg/ml PMMA added in the precursor showing a phase separation.

Table 3.1 Photovoltaic Parameters of Devices with PMMA in CB Antisolvents

PMMA (mg/ml)	V_{OC} (V)	J_{SC} (mA/cm²)	FF (%)	PCE (%)
Control	0.69	10.78	38.93	2.89
3.0	0.70	15.00	45.09	4.71
6.0	0.73	14.64	50.09	5.36
9.0	0.71	16.12	48.69	5.59

As shown in Table 3.1, main improvements in J_{sc} and FF led to significantly higher PCE. However, even though we have mitigated the negative impact of the polymer additive, some phase separation was still possible inside the film. Additionally, the polymer additive did not address the challenge of 2D/3D mixed perovskite solar cells, which is the quantum confinement brought by the mixed 2D/3D structure. We explored another additive that should has less impact on film fabrication and can change the phase distribution.

3.2 Anion-π Interactions for Phase Distribution Control

It is known that the formation energy of low-dimensional perovskite is significantly higher than 3D perovskites, which makes the competitive growth at low temperature become 3D dominant. According to this, we can divide the annealing process to two separate stages, one with

low temperature and another one with high temperature. This is called the gradient thermal annealing (GTA) method [3].

Table 3.2 Photovoltaic Parameters of Devices with GTA Method.

GTA Treatment	V_{OC} (V)	J_{SC} (mA/cm²)	FF (%)	PCE (%)
Control	0.69	10.78	38.93	2.89
30℃ 5 min, 70℃ 5 min	0.69	10.13	54.97	3.82
40℃ 5 min, 70℃ 5 min	0.71	9.86	58.34	4.09
50℃ 5 min, 70℃ 5 min	0.70	9.92	57.86	4.00

As shown in Table 3.2, the GTA method showed significant improvement in FF. Since it has been proven to form more high-n 2D phases and less multiple-quantum well structure, this brings the question: is there an additive can achieve a similar effect easily?

The hexafluorobenzene (HFB) molecule contains six electron-withdrawing fluorine atoms, imparting a strong positive quadrupole moment and notable π-acidity. It is hypothesized that HFB can form donor-acceptor interactions with iodide-containing species such as FAI and PEAI in the precursor. These interactions may retard the reactions between FAI and SnI_2, leading to slower and more controlled crystallization of tin perovskites. In addition, the strong electronegative fluorine group can form strong hydrogen bonding with PEA^+. These interactions with PEAI may restrict its diffusion during film formation, allowing more complete growth of higher-n 2D perovskite phases before low-n (e.g., n = 1) phase nucleation occurs. This effect is particularly relevant in quasi-2D systems where phase evolution is highly time-sensitive. Notably, HFB is volatile and expected to leave the film upon mild annealing (~70 °C), avoiding long-term incorporation into the final perovskite lattice and minimizing potential disruption to the electronic structure.

3.2.1 Investigation of HFB and Precursors Interactions via UV-Vis Spectroscopy

To validate the interaction of HFB with key precursor species, solution-phase UV-Vis spectroscopy was conducted. In the presence of HFB, PEAI and FAI solutions exhibited noticeable

redshifts in their absorption peaks, confirming donor-acceptor interactions. However, SnI_2 did not show a clear shift, suggesting that its interaction with HFB is either weak or negligible. This specificity in binding supports the selective modulation of organic components within the precursor matrix. These findings underscore the importance of tailoring molecular interactions within the precursor solution to guide the subsequent crystallization process.

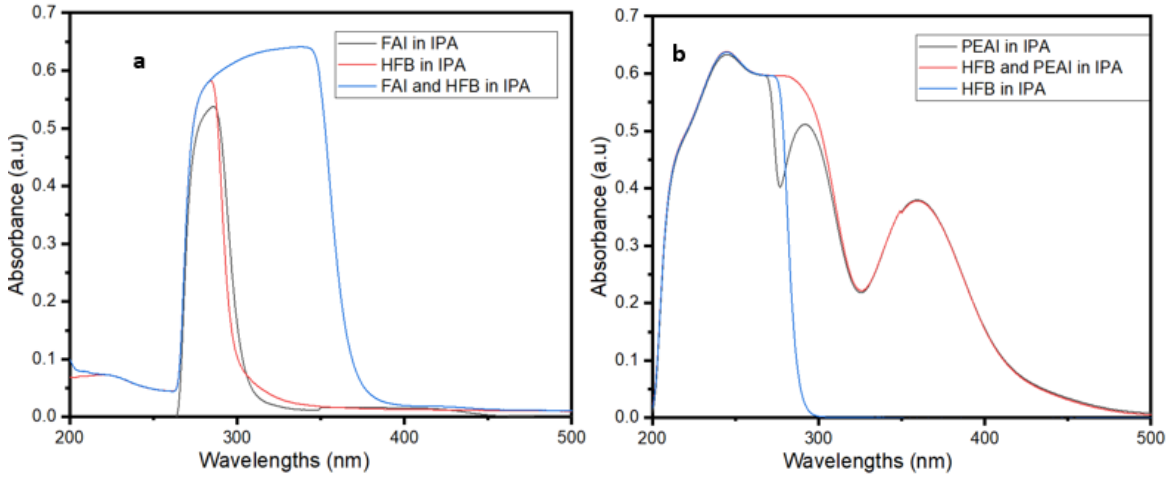

Figure 3.2 Solution UV-Vis data testing interactions between HFB and a) PEAI and b) FAI in IPA, respectively.

3.2.2 HFB Incorporated in Perovskite Precursors

To explore the effect of directly adding HFB into the precursor solution, films with increased quasi-2D content ($PEA_2FA_4Sn_5I_{16}$) were prepared using various of HFB concentrations (5, 15, and 25 µl/ml). UV-Vis absorption spectra revealed a decrease in n = 1 phase intensity and an increase in n = 2 features with higher HFB content. However, Ex-situ grazing incidence wide-angle X-ray scattering (GIWAXS) analysis on standard 15% PEAI films showed minimal change in low-n Bragg peaks, suggesting that in practical device fabrication, the effect of HFB in the precursor is relatively moderate. The limited change in structural signatures may be due to the non-uniform distribution of HFB or insufficient interaction timescales during film formation.

Device performance measurements aligned with these trends. Devices with 25 µl/mL HFB in the precursor exhibited a J_{sc} increase from 15.34 to 17.03 mA/cm², possibly attributed to reduced charge-blocking n=1 phases. Moderate improvements in V_{oc} and FF were also observed, likely due to enhanced film uniformity and reduced recombination losses. However, the limited GIWAXS n = 2 peak signal change doesn't suggest the corresponding performance improvement. This could be possibly resulted from the reduced n=1 phase, which is invisible in the GIWAX image. The n=2 peak signal remains almost unchanged.

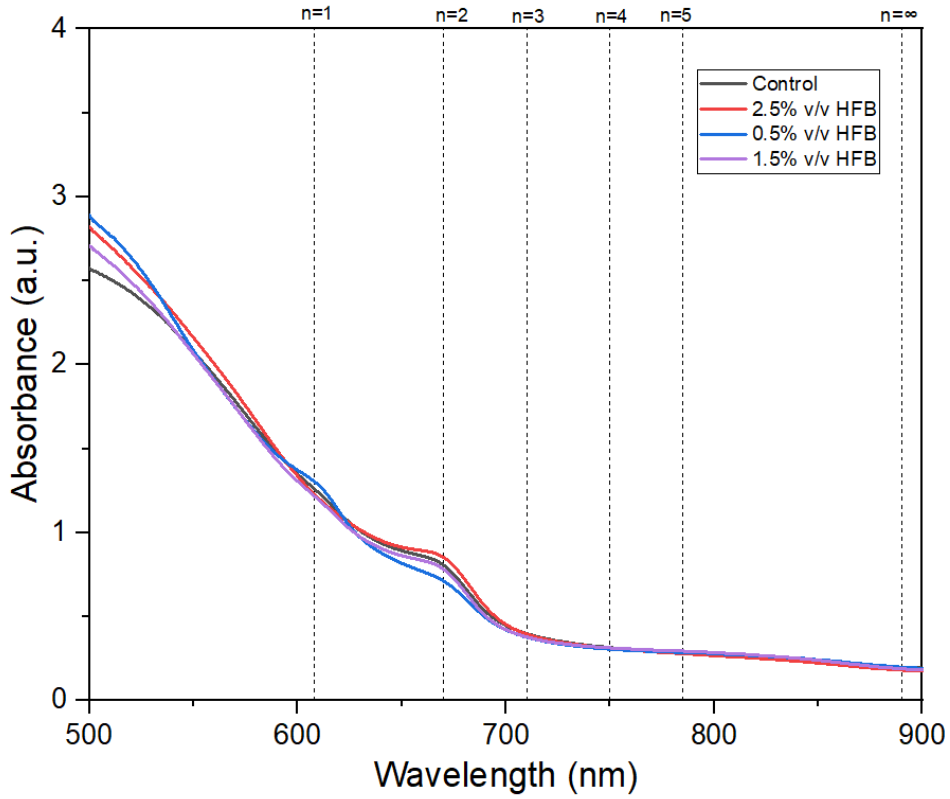

Figure 3.3 UV-Vis spectra on $PEA_2FA_4Sn_5I_{16}$ films with 5, 15, and 25 µl/ml HFB in precursor.

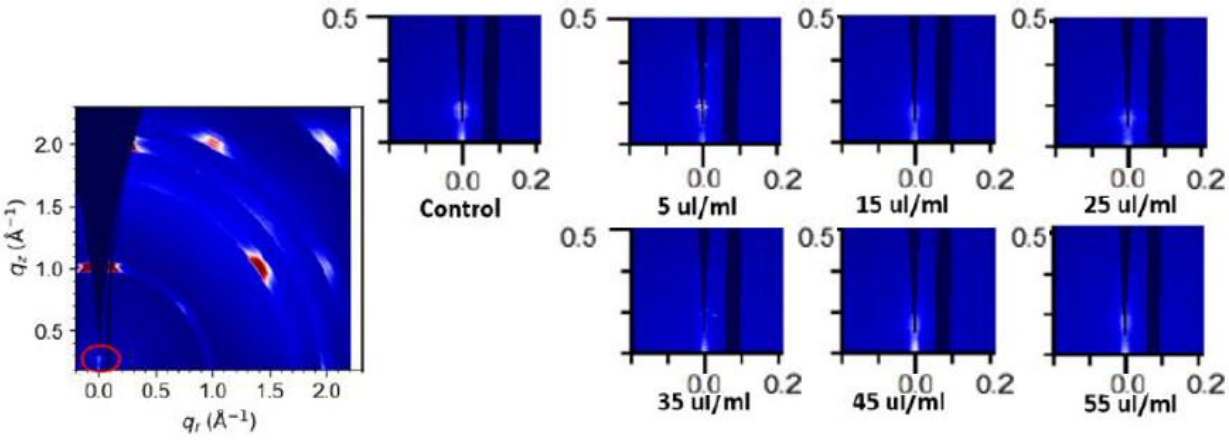

Figure 3.4. GIWAXS patterns of control film (15% PEAI) and enlarged n = 2 Bragg spots (q = 0.28) for films with different HFB concentrations in the precursors (Incident angle=0.5°).

Table 3.3 Device Performance of HFB Added in Precursors

HFB (µl/mL)	V_{OC} (V)	J_{SC} (mA/cm²)	FF (%)	PCE (%)
Control	0.47 ± 0.01	15.34 ± 1.00	60.59 ± 3.80	4.33 ± 0.24
5	0.44 ± 0.01	16.58 ± 0.63	58.90 ± 1.07	4.27 ± 0.31
15	0.44 ± 0.03	16.65 ± 0.47	59.89 ± 1.45	4.42 ± 0.41
25	0.44 ± 0.05	17.03 ± 0.79	57.25 ± 6.56	4.32 ± 1.02
35	0.45 ± 0.01	14.00 ± 1.06	61.49 ± 1.99	3.88 ± 0.36
45	0.50 ± 0.01	12.63 ± 1.16	66.09 ± 2.28	4.12 ± 0.11
55	0.47 ± 0.01	14.56 ± 1.05	63.54 ± 1.45	4.32 ± 0.14
65	0.41 ± 0.01	15.34 ± 0.79	57.32 ± 2.99	3.62 ± 0.35
75	0.41 ± 0.01	14.57 ± 1.20	60.40 ± 1.59	3.64 ± 0.39

3.2.3 HFB Delivered through Antisolvent

Recognizing the limitations of precursor-based HFB incorporation, HFB was also introduced through the antisolvent (chlorobenzene) during spin coating. GIWAXS data revealed a much stronger enhancement in n=2 phase formation, with 25 µl/ml HFB yielding the clearest increase in n=2 Bragg intensity. This was accompanied by a more pronounced J_{sc} improvement from 16.24 to 19.41 mA/cm². The more significant structural changes observed in GIWAXS

suggest more direct participation of HFB in the nucleation and growth process when delivered during crystallization.

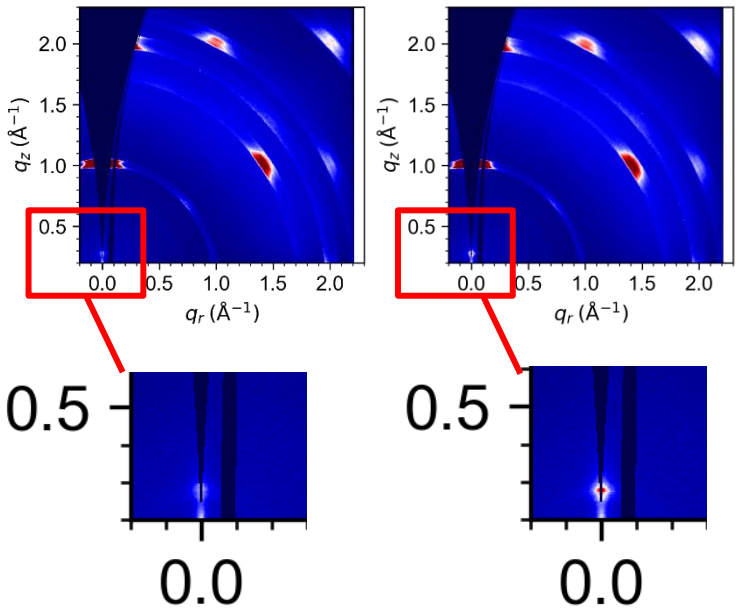

Figure 3.5. GIWAXS patterns and enlarged portion showing n = 2 spot for the tin perovskite films with 0 (left) and 25 µl/ml (right) HFB added in antisolvents (Incident angle=0.5°).

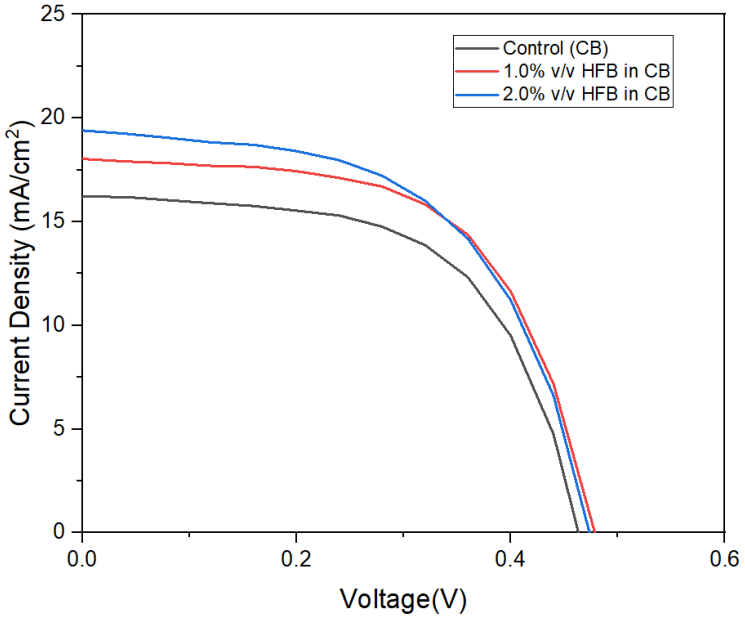

Figure 3.6 J-V characteristics of tin PSCs fabricated with the active layers with HFB added in antisolvents

Table 3.4 Device Performance of HFB Added in Antisolvents

HFB (µl/mL)	V_{OC} (V)	J_{SC} (mA/cm²)	FF (%)	PCE (%)
Control	0.46	16.24	58.88	4.39
10	0.47	18.04	59.00	5.04
20	0.47	19.41	55.95	5.08

The improved performance when HFB was delivered via antisolvent is likely due to its direct participation in the tin perovskite's fast crystallization process, promoting selective inhibition of n=1 phase growth. Additionally, HFB could avoid clustering in the precursor by bypassing exposure in the precursor solution. This approach ensures improved additive participation and minimizes loss due to volatility prior to film formation.

3.3. Other precursor additives

Several precursor additions were tried on the perovskite film to improve its performance. First, Br^- is known to change the tin perovskite's energy band structure. MA^+ as cation

substitution can promote highly oriented growth[4]. NH_4SCN is known to be effective in tin perovskite solar cells mainly by coordination between SCN^- and the perovskite network[5]. Guanidinium is known to improve the tin perovskite crystal growth, both as precursor addition and bottom surface treatment.[6][7]

The addition of 15% methylammonium bromide (MABr) shows a sharp improvement on V_{oc}, which meets the expectation of a better energy alignment by expanding the perovskite's bandgap. 13% ammonium thiocyanate (NH_4SCN) seems to be the optimum concentration, raising the V_{oc} from 0.392 V to 0.503 V, and also the fill factor increased by 10%. 30% addition of guanidinium thiocyanate (GASCN) is also effective on V_{oc} and fill factor improvement, but was less stable in performance, probably due to the high concentration. The pseudo-halide BF^{4-} was expected to achieve a similar effect as NH_4SCN, but it didn't improve the performance. NH_4BF_4 powder seems to change the powder color. This could happen because of some ion exchange between precursor components or simply because the NH_4BF_4 is polluted.

Table 3.5 Device Performance of Different Precursor Additives

Additives	**V_{OC} (V)**	**J_{SC} (mA/cm²)**	**FF (%)**	**PCE (%)**
Control	0.39	15.08	57.26	3.38
15% MABr	0.54	14.18	61.23	4.67
6.5% NH_4SCN	0.50	12.42	69.72	4.30
13%NH_4SCN	0.50	14.95	67.28	5.06
15% GASCN	0.50	11.70	66.34	3.89
30% GASCN	0.48	13.75	70.48	4.65
10% NH_4BF_4	0.81	5.20	40.49	1.69
6.67% NH_4BF_4	0.82	7.38	42.76	2.56

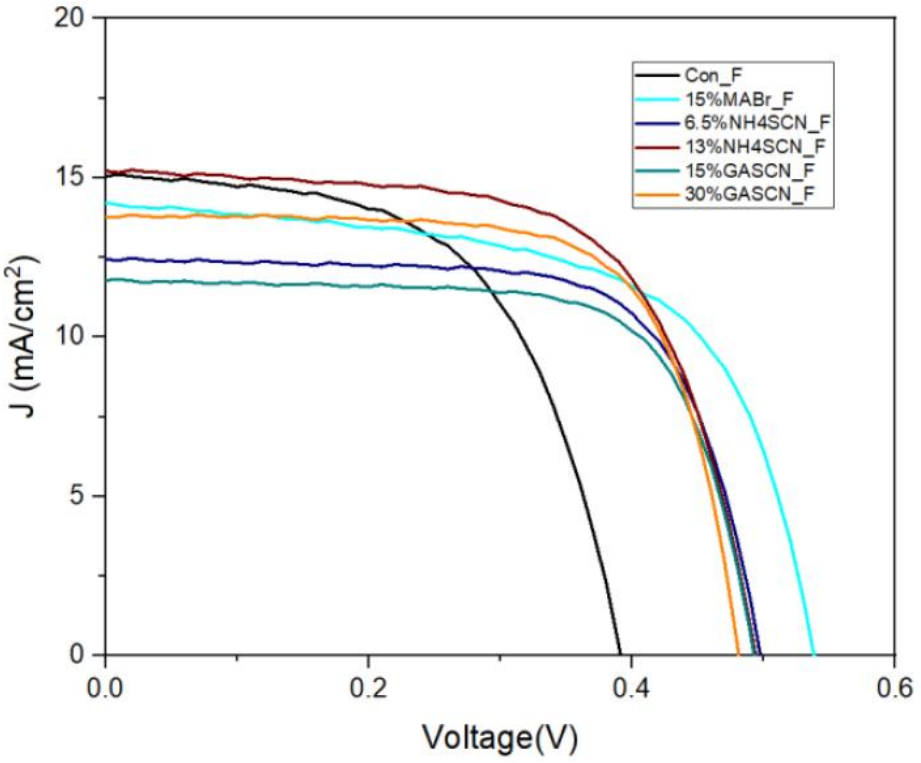

Figure 3.7 J-V characteristics of other tested additives

3.4. Conclusion

This study demonstrates that HFB can serve as a functional additive to modulate low-n phase content in quasi-2D tin perovskites. When added to the precursor, HFB mildly shifts the phase distribution towards higher-n configurations, resulting in modest performance gains. More pronounced effects are observed when HFB is applied via antisolvent, likely due to improved interaction with the crystallizing interface and avoidance of solution-phase aggregation. These results suggest that non-covalent molecular engineering strategies such as anion-π interactions can play a significant role in guiding perovskite phase behavior and improving optoelectronic properties.

CHAPTER 4

Interfacial Engineering via Spacer Ligands and Electron Transport Materials

Charge recombination, accumulation, and interface mismatch are preferred to happen more at both the bottom (HTL/perovskite) and top (perovskite/ETL) interfaces, since there are more defects. A dual-sided strategy targeting both interfaces is expected to show significant improvements on device performance. Thus, Chapter 4 focuses on interfacial engineering—including both bottom and top surfaces—using a combination of low-dimensional ligand treatments and interfacial interlayers to maximize charge extraction efficiency and minimize recombination losses.

4.1 Self-Assembled Monolayers (SAMs)

The performance of tin-based perovskite solar cells (TPSCs) has improved steadily. However, most high-efficiency devices still rely on PEDOT: PSS as the hole-transport material (HTM), despite its physical limitations. PEDOT: PSS is hygroscopic and unstable under long illumination, often leading to degraded performance. Replacing it with self-assembled monolayers (SAMs) offers advantages such as enhanced chemical stability, improved energy alignment, and more compact, inert interfaces. While SAMs are widely used in lead-based PSCs, their application in tin-based quasi-2D systems remains underexplored.

PEDOT: PSS, though popular as a hole transport layer in inverted PSCs, has some significant drawbacks. Its moisture sensitivity promotes degradation of tin perovskites, especially under long light exposure time. SAMs present a more stable and inert alternative, forming interfaces that are more suited to tin systems. An effective SAM typically includes: (1) an electron-withdrawing anchoring group to bind the ITO or FTO surface, (2) an electron-donating end-group to facilitate hole extraction, and (3) a stable linker to ensure proper alignment and packing. SAMs can be deposited by spin coating or dipping. Dipping method immerses the substrate in a dilute SAM solution for self-assembly, while spin coating allows quicker deposition.

4.1.1 Mixed SAM Strategy for Improved Wettability and Film Coverage

The MeO-2PACz molecule is commonly used as the SAM for its favorable energy alignment with tin perovskites. However, its hydrophobic nature significantly limits precursor wetting and leads to non-uniform coverage. To address this, a binary SAM system composed of MeO-2PACz and 6-phosphonohexanoic acid (6PA) is introduced [8]. The addition of 6PA provides hydrophilic functionality and improves the wettability, thereby promoting better precursor spreading and continuous film formation.

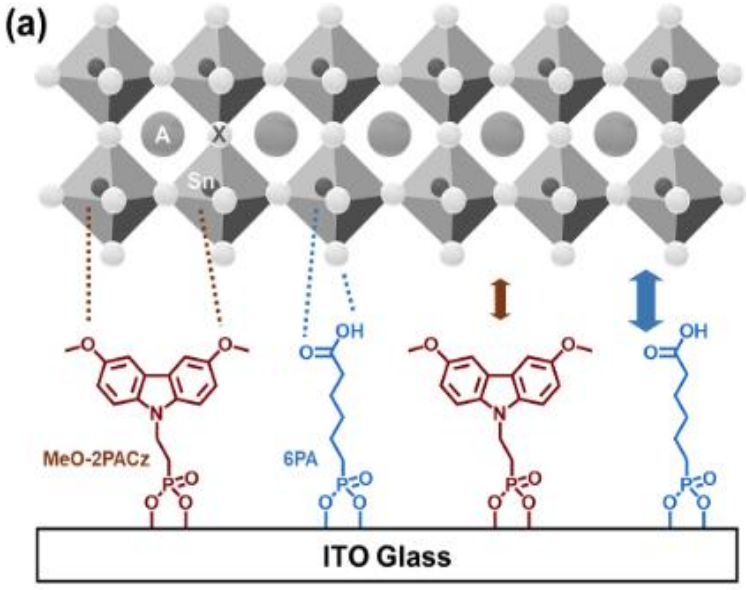

Figure 4.1 Illustration of the mixed SAM strategy [8]

Contact angle measurements confirm enhanced wetting behavior upon co-deposition of MeO-2PACz and 6PA. Subsequent spin coating of quasi-2D perovskite precursor solutions led to visually smoother films with reduced pinhole density. However, despite morphological improvements, the resulting devices exhibited pronounced S-shaped J–V curves and reduced power conversion efficiencies compared to PEDOT: PSS-based control devices. This indicates that while mixed SAMs improve surface wetting, other interfacial issues—possibly related to energy level mismatch or excessive surface dipole effects—may still dominate charge extraction behavior.

4.1.2 Post-deposition Solvent Rinse to Remove Excess SAM Molecules

To further investigate the impact of SAM surface coverage on device performance, a post-deposition rinse step was introduced to remove excess or loosely bound SAM molecules. Two solvents with differing polarity and miscibility—ethanol and DMF—were tested. Ethanol rinsing slightly enhanced device performance, notably increasing J_{sc} and stabilizing V_{oc}, suggesting that removal of excessive molecules reduces interfacial recombination sites without disrupting the covalently bound monolayer.

In contrast, DMF rinsing induced a marked decrease in both V_{oc} and FF. This may be attributed to the partial removal or disordering of the SAM layer due to its higher solvation strength. These results underscore the importance of gentle, selective rinsing to tune the interface quality in SAM-integrated devices.

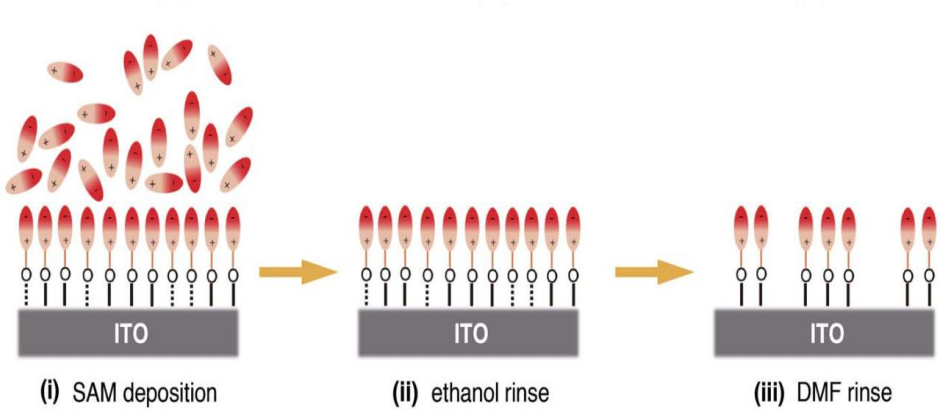

Figure 4.2 Illustration of post-deposition solvent rinse [9]

Table 4.1 Effect of Post-deposition Solvent Rinse on Device Performance

Hole Transport Layer	V_{OC} (V)	J_{SC} (mA/cm²)	FF (%)	PCE (%)
Co-SAM	6.34	0.51	57.97	1.87
Co-SAM (DMF rinsed)	9.18	0.45	41.42	1.70
Co-SAM (Ethanol rinsed)	7.01	0.51	56.25	1.99

4.1.3 Light Soaking and S-shaped J–V Curve

A unique phenomenon observed across all SAM-based devices is the evolution of the J–V curve shape upon continuous illumination. Initially, devices exhibit strong S-shape distortion characterized by low FF and suppressed current density. However, after a few minutes of light soaking, the J–V curve transitions to a more ideal diode shape, with increased V_{oc} and FF but reduced J_{sc}. After few minutes of resting in dark, the sample J-V characteristics go back to S-shaped. Such reversible transformation of J-V characteristic was never seen in PEDOT: PSS based devices.

According to the simulation data of a bilayer device with varied mobilities [10], such S-shaped J-V curve was likely caused by an imbalanced hole and electron transport across the device. Similar S-shaped J-V curve was witnessed in the simulation with one carrier mobility significantly higher than the other. From this, we can hypothesize that this S-shaped J-V behavior suggests the presence of imbalanced charge transport, and the reversible nature suggests the photo-induced trap filling or interfacial ion redistribution, which mitigates interfacial barriers over time. One plausible hypothesis is that rapid hole extraction through the SAM layer, coupled with sluggish electron transport through PCBM, leads to charge accumulation and interfacial field distortion. Illumination may assist in trap deactivation or interface dipole rearrangement, resulting in partial recovery of the built-in field and improved charge collection.

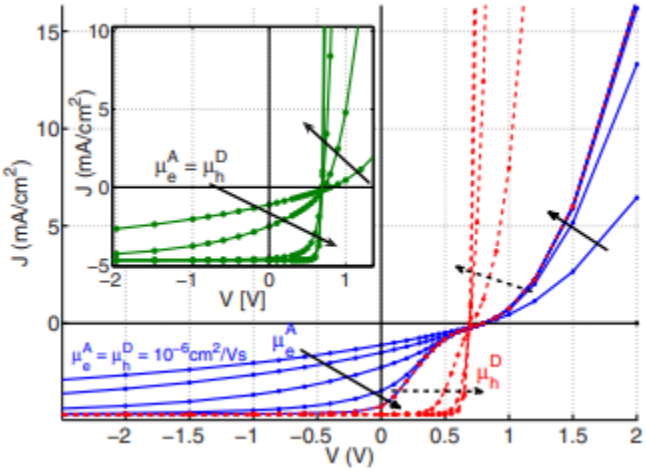

Figure 4.3. Simulation data of a bilayer device with varied mobilities. Solid lines: hole mobility in donor μ_h^D kept constant at 10^{-6} cm^2 /V s, with electron mobility in acceptor μ_e^A varied from 10^{-6} to 10^{-2} cm^2 /V s with an increment of 10^{-1} cm^2 /V s. Dashed lines: μ_e^A constant at 10^{-2} cm^2 /V s, with μ_h^D varied from 10^{-6} to 10^{-2} cm^2 /V s with the same increment. Inset: balanced mobilities $\mu_e^A = \mu_h^D = 10^{-6}$ to 10^{-2} cm^2 /Vs [10]

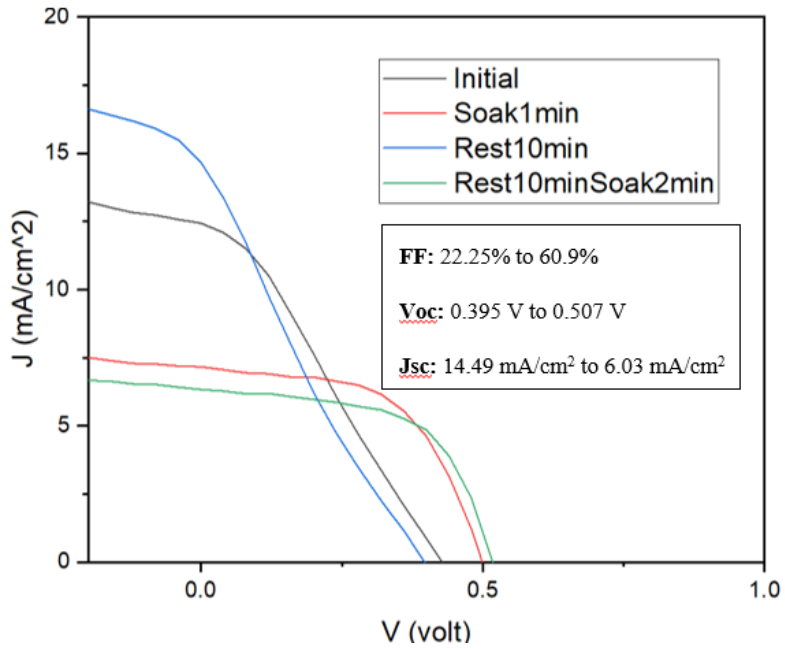

Figure 4.4 Effects of light soaking on co-SAM J-V characteristics

4.2. Bottom-Surface Modification via 2D Ligand Interlayers

The bottom interface plays a critical role in initiating oriented perovskite crystal growth and reducing trap-assisted recombination. To explore this, we implemented a low-dimensional perovskite (LDP) interlayer strategy by spin-coating organic spacer ligands directly onto PEDOT: PSS before deposition of the perovskite precursor. These ligands form thin 2D perovskite layers at the bottom of the film, serving to guide the vertical crystallization of perovskites and passivate interfacial defects.

Different ligands were tested, including 2-thioethylammonium iodide (2TEAI), phenethylammonium bromide (PEABr), 4-fluorophenethylammonium iodide (4F-PEAI), and phenethylammonium thiocyanate (PEASCN). Among these, PEABr and 4F-PEAI yielded the highest PCE values, particularly under non-annealed conditions. As shown in Table 4.2, ligands that were spin-coated without subsequent thermal annealing outperformed their annealed counterparts. This suggests that residual ligands at the interface may actively influence subsequent perovskite nucleation and promote vertical perovskite orientation.

Table 4.2 Organic Ligand Bottom Surface Treatment

Organic Ligands (20 mg/ml)	V_{OC} (V)	J_{SC} (mA/cm²)	FF (%)	PCE (%)
Control	0.51	16.15	60.59	4.92
PEASCN w/ Anneal	0.52	15.88	61.36	5.06
2TEAI w/ Anneal	0.53	17.45	61.83	5.72
4F-PEAI w/ Anneal	0.53	16.13	63.18	5.38
PEABr w/o Anneal	0.54	17.10	63.43	5.85
PEASCN w/o Anneal	0.51	16.05	65.78	5.39
2-TEAI w/o Anneal	0.50	13.89	65.46	4.49
4F-PEAI w/o Anneal	0.51	17.77	66.24	6.00

Devices treated with non-annealed PEABr exhibited a notable improvement in all photovoltaic metrics, achieving J_{sc} values exceeding 17.10 mA/cm², V_{oc} around 0.54 V, and FF of 63.43%. The performance enhancement is attributed to multiple factors: (1) enhanced crystallographic alignment enabled by the templating effect organic ligand on crystal orientation,

and (2) improved chemical interaction between ammonium headgroups and the PEDOT: PSS surface, leading to reduced trap densities.

In contrast, ligands like PEASCN and 2TEAI showed less pronounced improvements. PEASCN exhibited moderate increases in V_{oc} but limited gain in J_{sc}, likely due to poor wettability and less effective vertical phase alignment. 2TEAI did not significantly improve device performance, potentially due to excessive steric hindrance or weaker interaction with the substrate.

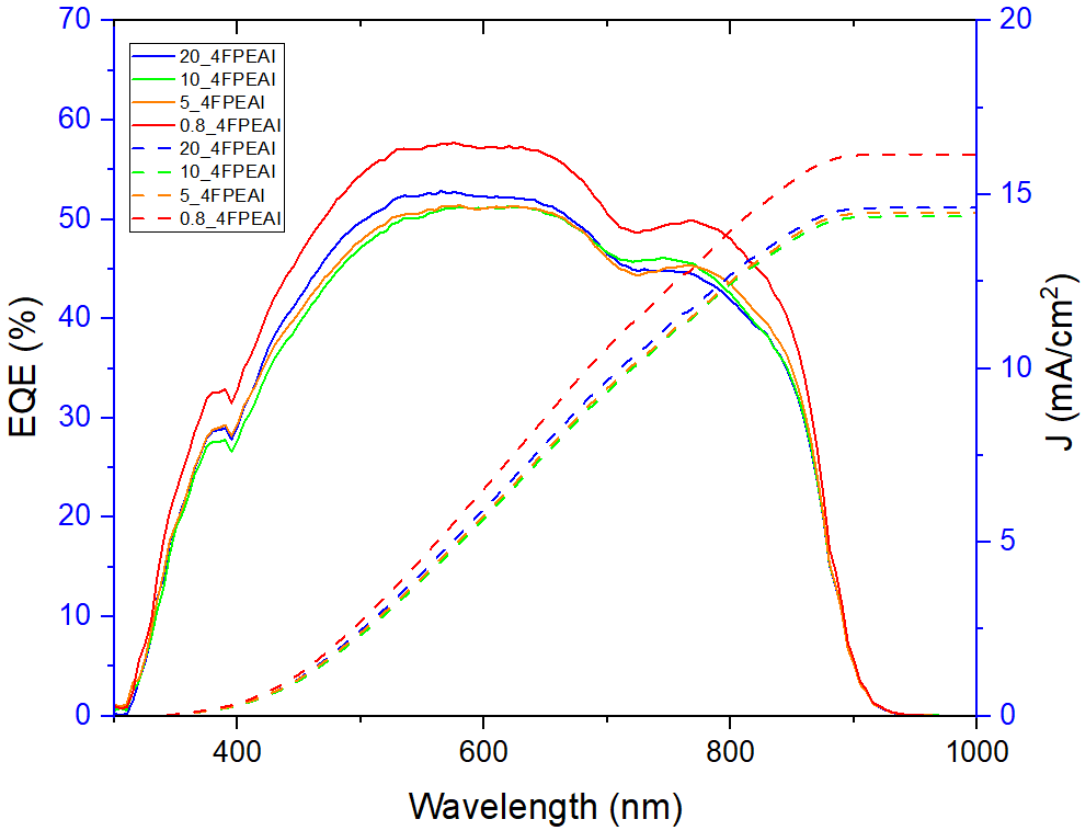

Figure 4.5 EQE spectra of 4FPEAI bottom treatment with different concentrations

However, after multiple batches of performance testing, the device treated with 4FPEAI was observed to exhibit the most stable performance across fabrication trials, even though its absolute improvement in efficiency was not the highest among the entries listed in the Table 4.2 To further investigate the influence of ligand concentration on device performance, we conducted EQE measurements on devices fabricated with varying concentrations of ligands applied to the bottom interface. In this context, 4FPEAI was selected as a representative case for detailed analysis.

Figure 4.5. shows the EQE spectra of devices treated with different concentrations of 4FPEAI. Among these, the device incorporating 0.8 mg/mL of 4FPEAI displayed noticeably higher absorption across the entire wavelength range compared to devices with either lower or higher ligand concentrations. Theoretically, ligands deposited at the bottom interface may participate in the early stages of perovskite crystallization, leading to the formation of thin two-dimensional perovskite layers near the substrate. These quasi-2D structures can negatively affect charge transport due to their inherent multiple quantum well characteristics, which tend to localize carriers and hinder their movement across the vertical direction.

Given that the precursor solution already contains 15% PEAI as a 2D spacer cation, the introduction of excessive additional ligand from the bottom surface may exacerbate this effect. The increased presence of low-dimensional phases likely impedes vertical charge transport throughout the device, providing a plausible explanation for the reduced absorption observed at higher ligand concentrations. These results collectively demonstrate the strong structure–property relationship between ligand composition and interfacial crystallization dynamics. Electron-withdrawing groups (such as fluorine in 4FPEAI) appear to modulate interface dipoles more effectively, contributing to superior band alignment and reduced recombination.

4.3 Top-Surface Modification

In parallel to bottom interface tuning, we examined top-side treatments to improve electron extraction and reduce surface recombination at the perovskite/ETL junction.

4.3.1 ICBA Surface Treatment

The concept of surface reconstruction was interesting. The perovskite film surface is highly defective. It is covered by defects like undercoordinated Sn^{2+} ions and Sn^{2+} vacancies, accelerating the Sn^{2+} oxidation and nonradiative recombination. Given the defective and fragile surface, interface engineering aimed at reducing the surface defects of $FASnI_3$ films is vital. Our initial attempts were using IPA or IPA-dissolved ligands to wash off the surface imperfections and ‘fix’ them with functional components in the solution. However, such method is not practical in this case since the IPA solvent can severely degrade the tin perovskite film due to solubility and incompatibility issues as shown in Figure 4.6. The destroyed perovskite film surface shows a

yellowish color and many visible pinholes. Since the tin perovskite is highly sensitive to various solvents, it is hard to apply similar methods. To avoid this, we employed ICBA, a fullerene derivative known for its favorable energy level alignment and solubility in chlorobenzene. Since chlorobenzene is used as the antisolvent for tin perovskite, it is a safe choice of solvent for surface treatments. ICBA is also widely used as the electron transport layer in perovskite solar cells, providing impressive records of performance when solely used as the ETL [11], so the surface treatment should be perfectly safe to the tin perovskite film itself.

Systematic studies were performed by spin-coating ICBA at different concentrations: 3, 6, 9, and 12 mg/mL, onto the perovskite surface prior to PCBM deposition. The performance exhibited a non-linear trend with concentration. Devices treated with 12 mg/mL ICBA achieved the best results, reaching a PCE of 6.03%, V_{oc} of 0.52 V, and J_{sc} of 17.84 mA/cm². At lower concentrations, performance gains were limited, and at excessively high concentrations, surface aggregation appeared to disrupt uniform film coverage.

These results indicate that ICBA serves as a dual-function additive, improving energy level alignment and passivating surface trap states. Its extended π-conjugation may also facilitate charge delocalization at the interface, contributing to smoother energy band transitions and reduced recombination.

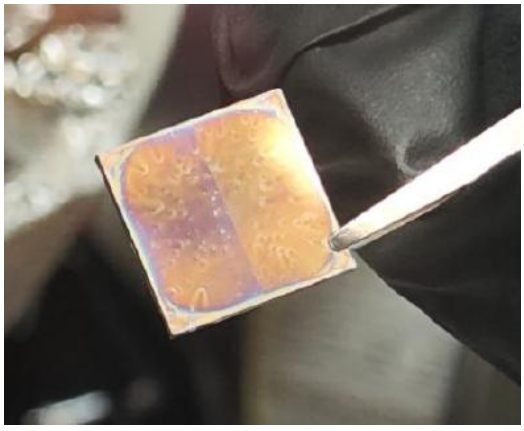

Figure 4.6 IPA surface treatment caused a destructed tin perovskite film

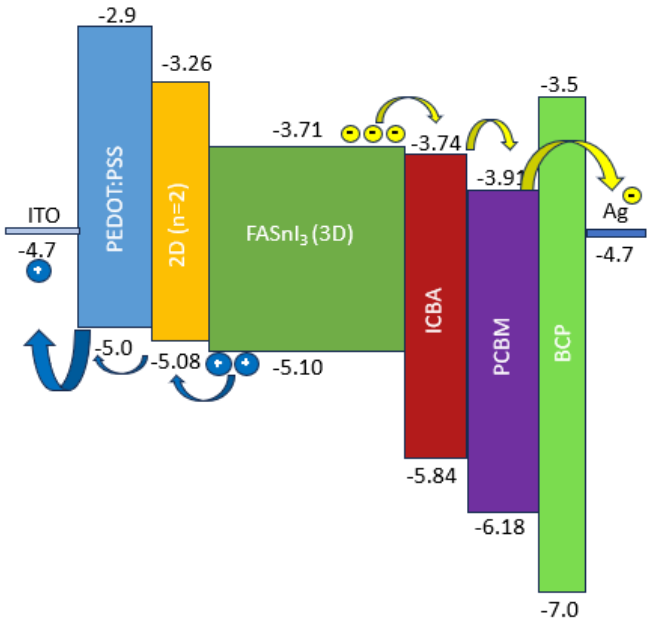

Figure 4.7 Illustration of improved band alignment by ICBA

Table 4.3 Different Concentrations of ICBA Surface Treatments

ICBA Surface Treatments (mg/ml)	V_{OC} (V)	J_{SC} (mA/cm²)	FF (%)	PCE (%)
Control	0.49	14.57	60.58	4.28
1.5	0.50	17.10	58.44	4.96
3	0.50	14.41	61.01	4.40
4.5	0.47	15.76	58.08	4.29
6	0.50	15.93	63.96	5.10
9	0.53	15.61	67.41	5.55
12	0.52	17.84	65.47	6.03
15	0.51	16.91	65.17	5.56

4.3.2 Mixed ETL Strategy: Co-deposition of ICBA and PCBM

Given the shared solvent compatibility and complementary properties of ICBA and PCBM, a co-deposition strategy was adopted to combine their advantages in a single-step deposition process. The rationale behind this approach lies in improving the energy level alignment (Fig. 4.7)

and potential surface passivation capabilities of ICBA, alongside the well-established electron transport characteristics of PCBM. Through precise control of component ratios within the solution, we aimed to construct a mixed electron transport layer (ETL) that could synergistically address interfacial energy alignment while maintaining continuous charge extraction pathways across the perovskite/ETL interface.

To systematically evaluate this concept, a series of molar compositions were investigated, specifically ICBA to PCBM volume ratios of 9:1, 7:3, and 5:5, each dissolved in chlorobenzene at controlled concentrations. The dropped solution volume was controlled to be the same. This design enabled a controlled examination of how a gradual increase in ICBA content modulates the resulting ETL film.

The co-deposition approach should allow the intermolecular packing and within the ETL and the surface passivation over the perovskite layer, both of which are known to influence carrier dynamics and reduce recombination losses. The goal of this investigation was not only to optimize charge mobility and energy level alignment independently, but to identify a compositional window in which both effects are maximized through synergy.

The optimal configuration was achieved with an ICBA/PCBM molar ratio of 0.20, corresponding to a 7:3 volume ratio of 15 mg/mL ICBA and 30 mg/mL PCBM. Devices fabricated with this blend exhibited a PCE of 7.25%, V_{oc} of 0.55 V, and J_{sc} of 20.12 mA/cm²—nearly double the current output of control devices. Morphological characterization revealed smoother film coverage and potentially favorable microphase separation, which could facilitate lateral charge transport pathways and reduce energy barriers at grain boundaries.

Table 4.4 Different Molar Ratios of ICBA/PCBM Mixed ETL Treatments

ICBA/PCBM Molar Ratio	V_{OC} (V)	J_{SC} (mA/cm²)	FF (%)	PCE (%)
Control	0.46	14.50	59.38	3.94
0.05	0.51	17.98	64.79	5.88
0.20	0.55	20.12	66.28	7.25
0.48	0.57	17.14	66.57	6.43

Figure 4.8. shows the EQE spectra of the control device employing PCBM as the electron transport layer (ETL) (red), the device utilizing a mixed ETL (green), and the device incorporating

both a mixed ETL and 4F-PEAI bottom surface treatment (blue). The device with the mixed ETL exhibits slightly reduced absorption in the low and medium wavelength ranges, but demonstrates a pronounced enhancement in absorption at longer wavelengths. Upon introducing the 4F-PEAI bottom treatment, absorption improves across the entire spectral range, although it still remains marginally lower than the control device in the medium wavelength region.

These EQE results suggest that the mixed ETL facilitates stronger absorption near the top surface of the perovskite layer, potentially attributed to more efficient charge extraction and reduced nonradiative recombination at the upper interface. Conversely, the slight reduction in absorption at shorter wavelengths may be a consequence of increased ETL thickness, which can hinder photon transmission into deeper regions of the active layer.

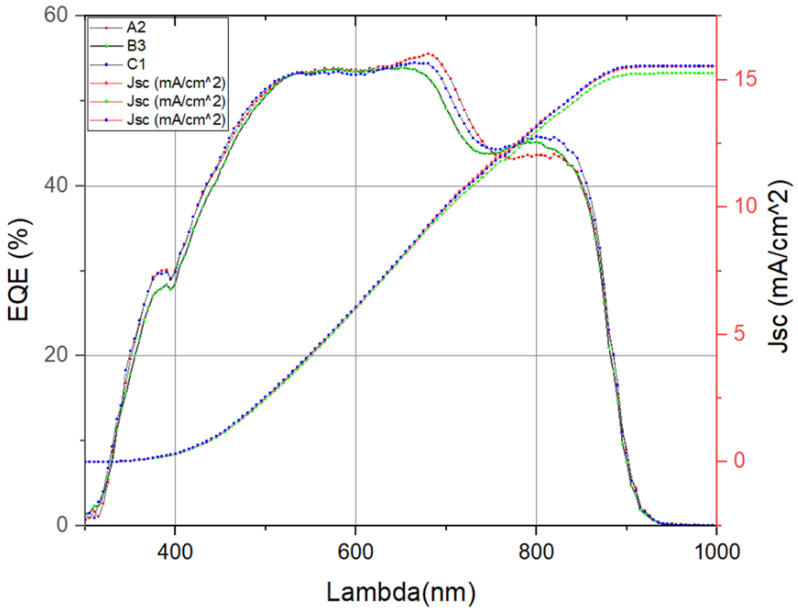

Figure 4.8. EQE spectra of control (red), mixed ETL (green, ICBA/PCBM=0.20), and 4FPEAI bottom treatment plus mixed ETL (blue, 20 mg/ml 4FPEAI spin-coated at 5000 rpm for 30s and annealed at 70°C for 10 min)

4.4. Conclusion

Chapter 4 demonstrates that targeted interfacial modifications at both the bottom and top of the perovskite layer significantly enhance device performance in quasi-2D tin PSCs. The bottom 2D interlayer promotes vertical crystal orientation and reduces charge carrier recombination, while

the ICBA top treatment and mixed ICBA/PCBM ETL enable more efficient electron extraction. Concentration optimization and ligand thermal history play crucial roles in defining the effectiveness of each strategy. Comparative studies of ligand chemistry underscore the importance of fine-tuning molecular structure and anchoring properties to modulate interface energetics and perovskite morphology. The resulting synergetic improvements push PCEs beyond 7%, reduce hysteresis, and improve device uniformity, establishing interfacial engineering as a critical design lever for future low-toxicity perovskite solar cells.

CHAPTER 5

CONCLUSION and FUTURE WORK

5.1. Conclusion

Tin-based perovskite solar cells (TPSCs), as an alternative to lead-based systems have challenges like fast crystallization kinetics, Sn^{2+} oxidation, inefficient charge extraction, and quantum confinement in mixed 2D/3D system. In this work, we have presented an integrated strategy that addresses these issues through both bulk material engineering and interfacial design, offering approaches to enhance the device performance.

In the perovskite film bulk, we explored the role of polymer and small-molecule additives in modulating crystallization behavior and controlling phase distribution. PMMA, as a polymer additive, demonstrated the potential to passivate defects and improve film uniformity when used in the antisolvent phase. However, it also shows a risk of phase separation when applied to the precursor. To overcome this, we turned to small molecules like HFB, which offered unique benefits through anion-π interactions. Delivered via antisolvent, HFB effectively changes the low-n phase distribution, leading to substantial improvements in J_{sc} and overall device performance. In addition, precursor additives such as MABr, NH_4SCN, and GASCN were investigated to fine-tune the electronic structure and crystallization environment. These additives yielded significant enhancements in V_{oc} and FF.

At the perovskite interfaces, we engineered both the bottom and top surfaces of the perovskite absorber to reduce recombination and improve charge transport. Bottom-surface treatments using low-dimensional organic ligands such as 4F-PEAI created templated interfaces that improved vertically oriented growth and reduced interfacial defects. Among various ligands tested, 4F-PEAI stood out for its reproducibility and favorable optoelectronic characteristics. At the top interface, the use of ICBA as a surface treatment provided improved energy level alignment and passivation of surface traps, leading to improved electron extraction. Furthermore, co-deposition of ICBA with PCBM created a mixed electron transport layer that synergistically combined the advantages of both materials. The resulting devices showed record J_{sc} values over 20 mA/cm^2 and a peak PCE exceeding 7%.

5.2. Future Work

While this study presents effective strategies for improving tin-based perovskite solar cells, several directions remain open for further investigation. The role of HFB in modulating low-dimensional phases, though promising, requires a deeper understanding, particularly regarding its actual interaction mechanisms. Though its volatile nature avoids negative effects during crystallization, an alternative chemical with stronger and more stable positive effects on crystallization should be more ideal. For bottom-surface engineering, the influence of ligands like 4FPEAI on crystal orientation and defect formation requires further in-situ characterization to confirm the mechanisms. On the top side, exploring other fullerene derivatives and their change over co-deposition could further enhance electron extraction and stability. Additionally, the device stability requires further optimization. Improving long-term device stability through better perovskite recipe optimization and interfacial protection will be essential for higher device performance.

REFERENCE

[1] Abdulkarim AS, Srivastava M, Ngulezhu T, Singh D, Strzałkowski K, Singh RC, Yahya MZ, Yusuf SN, Diantoro M. An overview of tin based perovskite solar cells: Stability and efficiency. Current Applied Physics. 2025 Jan 15.

[2] Sun N, Gao W, Dong H, Liu Y, Liu X, Wu Z, Song L, Ran C, Chen Y. Architecture of pin Sn-based perovskite solar cells: characteristics, advances, and perspectives. ACS Energy Letters. 2021 Jul 26;6(8):2863-75.

[3] Yao H, Wu T, Xiao Y, Ding L, Hua Y, Hao F. Regulating the crystallization and carrier dynamics for High-Performance Quasi-2D Tin perovskite solar cells. ACS Materials Letters. 2023 Nov 6;5(12):3203-11.

[4] Yu BB, Liao M, Zhu Y, Zhang X, Du Z, Jin Z, Liu D, Wang Y, Gatti T, Ageev O, He Z. Oriented crystallization of mixed-cation tin halides for highly efficient and stable lead-free perovskite solar cells. Advanced Functional Materials. 2020 Jun;30(24):2002230.

[5] Li W, Ding S, Xu J, Wu C, Li X, Qian L, Chen H, Zhang X, Kang K, Xiang C. Ammonium Thiocyanate Enhanced High-Performance Quasi-Two-Dimensional Perovskite Solar Cells. ACS Applied Energy Materials. 2024 Jan 31;7(3):1120-7.

[6] Zhou Y, Yan D, Feng X, Shen B, Yang L, Wang J, Chen R, Lv W, Xu L. Buried Interface Modification via Guanidine Thiocyanate for High-Performance Lead-Free Perovskite Solar Cells. The Journal of Physical Chemistry C. 2023 Jan 13;127(3):1320-5.

[7] Wang T, Loi HL, Cao J, Qin Z, Guan Z, Xu Y, Cheng H, Li MG, Lee CS, Lu X, Yan F. High Open Circuit Voltage Over 1 V Achieved in Tin-Based Perovskite Solar Cells with a 2D/3D Vertical Heterojunction. Advanced Science. 2022 Jun;9(18):2200242.

[8] Song D, Ramakrishnan S, Zhang Y, Yu Q. Mixed self-assembled monolayers for high-photovoltage tin perovskite solar cells. ACS Energy Letters. 2024 Mar 12;9(4):1466-72.

[9] Tang H, Shen Z, Shen Y, Yan G, Wang Y, Han Q, Han L. Reinforcing self-assembly of hole transport molecules for stable inverted perovskite solar cells. Science. 2024 Mar 15;383(6688):1236-40.

[10] Tress W, Petrich A, Hummert M, Hein M, Leo K, Riede M. Imbalanced mobilities causing S-shaped IV curves in planar heterojunction organic solar cells. Applied Physics Letters. 2011 Feb 7;98(6).

[11] Lee M, Kim D, Lee YK, Koo H, Lee KT, Chung I. Indene-C60 bisadduct electron-transporting material with the high LUMO level enhances open-circuit voltage and efficiency of Tin-based perovskite solar cells. ACS Applied Energy Materials. 2020 May 6;3(6):5581-8.